JOURNAL OF CATALYSIS 138, 588–610 (1992)

Non-Faradaic Electrochemical Modification of Catalytic Activity

6. Ethylene Epoxidation on Ag Deposited on Stabilized ZrO_2

S. BEBELIS AND C. G. VAYENAS[1]

Institute of Chemical Engineering and High Temperature Chemical Processes, and Department of Chemical Engineering, University of Patras, Patras GR 26110, Greece

Received January 27, 1992; revised May 18, 1992

It was found that the catalytic activity and selectivity of polycrystalline Ag for the epoxidation and complete oxidation of C_2H_4 can be affected in a pronounced and reversible manner by electrochemically supplying or removing oxygen ions O^{2-} to or from the Ag catalyst surface via ZrO_2 (8 mol% Y_2O_3), an O^{2-} conducting solid electrolyte. The steady-state changes in the catalytic rates of formation of C_2H_4O and CO_2 are typically 5 to 50 times larger than the rate of O^{2-} transport to or from the catalyst surface; i.e., the reaction exhibits the effect of non-Faradaic electrochemical modification of catalytic activity (NEMCA). Under wide ranges of experimental conditions, the catalytic rates of C_2H_4O and CO_2 formation depend exponentially on catalyst potential and work function. The corresponding activation energies are linearly related to catalyst potential and work function with slopes close to -1. The selectivity to C_2H_4O can be very significantly decreased, but only moderately increased relative to open-circuit conditions. The observed phenomena are discussed and interpreted within the framework of previous NEMCA studies, some independent earlier *in situ* XPS observations, and the currently prevailing ideas regarding the mechanism of ethylene epoxidation. © 1992 Academic Press, Inc.

INTRODUCTION

The silver-catalyzed epoxidation of ethylene is a reaction of great technological importance. It also represents one of the most challenging and thoroughly studied catalytic systems (*1, 2*). Extensive research has been carried out so far, aiming toward both an increase in the selectivity to ethylene oxide and a fundamental understanding of the underlying catalytic chemistry. Work prior to 1987 has been reviewed by van Santen and Kuipers (*1*).

Most industrial reactors operate currently with a selectivity near 80%. The catalyst consists of reduced Ag particles dispersed on α-Al_2O_3. Alkalis are added to the catalyst as a promoter and chlorine compounds are added to the gas feed as moderators. The role of promoters and moderators has been studied intensively in recent years (*3–10*). Despite substantial progress in this area no complete or unanimous conclusions have yet been reached.

It is currently generally accepted that atomic oxygen is the catalytically active surface oxygen species, as shown conclusively by the work of Lambert and co-workers in the early and mid-eighties (*11, 12*). The presence of subsurface oxygen is a necessary condition for obtaining high selectivity to ethylene oxide (*1, 11, 14*) while molecularly adsorbed oxygen is currently believed to be a spectator species (*1, 11–13*). It has been recently proposed that product selectivity is governed by the binding state of atomic oxygen (*1, 11*). Weakly bound oxygen coordinated to a Ag ion of high positive charge is expected to lead to epoxidation while strongly bound bridging oxygen is expected to attack C–H bonds and lead to nonselective oxidation. The effect of promoters and moderators on the binding state of adsorbed

[1] Present address: Department of Chemical Engineering, Yale University, New Haven, CT 06520.

0021-9517/92 $5.00
Copyright © 1992 by Academic Press, Inc.
All rights of reproduction in any form reserved.

atomic oxygen is still the focus of numerous studies (*1–10*).

Catalytic phenomena on metals can be both studied and influenced by the use of solid electrolyte cells. Work in this area prior to 1988 has been reviewed by Vayenas (*16*) and Stoukides (*17*). In the early eighties these authors (*18–21*) used a solid electrolyte cell of the type

$$C_2H_4, O_2, Ag|ZrO_2\ (8\ mol\%\ Y_2O_3)|Ag, O_2 \quad (1)$$

to study the epoxidation of ethylene on a porous Ag catalyst film, which also served as an electrode. They used the cell both in a "passive" (*20*) and in an "active" mode (*18, 19*): first by measuring *in situ* the surface oxygen activity via the measurement of the open-circuit cell potential values (*20, 21*) and second by applying currents and voltages to the cell with a concomitant supply or removal of O^{2-} to or from the catalyst through the gas-impervious solid electrolyte (*18, 19*). Non-Faradaic behavior was observed; i.e., the steady-state rates of epoxidation and complete oxidation were found to change reversibly by up to a factor of 300 more than the steady-state rate of supply or removal of O^{2-}, which is $I/2F$, where I is the applied current and F is Faraday's constant. This suggested significant and reversible changes in the catalytic properties of the Ag catalyst films. Changes in product selectivity were also observed (*18, 19*) but, due to the lack of a reference electrode, catalyst potential and overpotential could not be measured.

The results of this early exploratory study (*18, 19*) can now be understood within the frame of the recently found effect of non-Faradaic electrochemical modification of catalytic activity (NEMCA) which has been studied so far for more than 20 catalytic reactions on Pt, Ni, Rh, Ag, Pd, and Au surfaces and utilizing both O^{2-}-conducting and Na^+-conducting solid electrolytes (*22–37*). The NEMCA literature has been reviewed in a recent monograph (*37*). The NEMCA effect, for which the term "electrochemical promotion in catalysis" has also been proposed (*38*), can be described as follows: A porous thin (typically 2–20 μm thick) metal catalyst film is deposited on a solid electrolyte as shown in Fig. 1 and a galvanostat or potentiostat is used to supply or remove ions to or from the catalyst surface at a rate $G = I/nF$, where n is the ion charge and I is the applied current-defined positive when anions are supplied to the catalyst. The current is applied between the catalyst and a counter electrode, usually exposed to a reference gas, while monitoring or controlling the ohmic-drop-free catalyst potential V_{WR} with respect to a reference electrode (*22–37*).

The induced change Δr in the catalytic rate can be up to a factor of 3×10^5 higher than the rate G of ion supply or removal and up to a factor of 70 higher than the unperturbed, i.e., open-circuit, catalytic rate r_o (*22–37*). The enhancement factor Λ is defined from

$$\Lambda = \Delta r/(I/nF). \quad (2)$$

A reaction exhibits the NEMCA effect when $|\Lambda| > 1$. When $\Lambda > 1$ the reaction is termed electrophobic, while when $\Lambda < -1$ the reaction is termed electrophilic (*22, 33, 37*).

The NEMCA effect can be explained by taking into account the induced change in the average work function $e\Phi$ of the gas-exposed catalyst surface as a result of the electrochemically induced spillover of ions onto the catalyst surface (*22, 25, 32*) and of the concomitant controlled change in the strength of chemisorptive bonds (*22, 25, 37*).

Theoretical analysis (*25, 26, 30, 37*) as well as recent experiments utilizing a Kelvin probe (*22, 32*) have confirmed that the induced change in catalyst work function $e\Phi$ is equal to $e\eta$, where $\eta = \Delta V_{WR}$ is the catalyst activation overpotential. The presence of activation overpotential denotes a "difficulty" in charge transfer at the gas–electrolyte–catalyst three-phase boundaries. This gives rise to the creation of charged or par-

tially charged species (e.g., O^{2-}, Na^+) which spill over onto the catalyst surface, together with their compensating image charge in the metal, altering the average work function of the gas-exposed catalyst surface.

This electrochemically induced doping of the catalyst surface results not only in dramatic changes in catalytic activity, but also in significant (and to a large extent predictable) changes in the strength of chemisorptive bonds. This was demonstrated recently for oxygen chemisorption on Ag where it was shown that decreasing the catalyst work function via oxide ion removal causes a sixfold increase in the sticking coefficient of oxygen and a twofold increase in the amount of reactive atomically bonded oxygen (*36*).

The electrochemically induced ion spillover and concomitant work function change can explain adequately all the general features of NEMCA observed in all 20 catalytic systems studied so far.

(i) Over wide ranges of catalyst work function $e\Phi$ (0.1–1 eV) catalytic rates depend exponentially on $e\Phi$:

$$\ln(r/r_o) = \alpha e(\Phi-\Phi^*)/k_bT. \quad (3)$$

Over the same $e\Phi$ (or equivalently eV_{WR}) ranges catalytic activation energies usually vary linearly with $e\Phi$.

(ii) The order of magnitude of the absolute value $|\Lambda|$ of the enhancement factor Λ can be estimated from

$$|\Lambda| \approx 2Fr_o/I_0, \quad (4)$$

where I_0 is the exchange current of the catalyst–solid electrolyte interface.

(iii) The reaction rate relaxation time constant τ during galvanostatic transients, defined as the time required for the rate change to reach 63% of its final steady-state value when a constant current is applied between the catalyst and the counter electrode, can be approximated by

$$\tau \approx nFN/I, \quad (5)$$

where N, expressed in metal g-atom, is the gas-exposed catalyst surface area. This implies that NEMCA is a catalytic effect taking place over the entire catalyst surface.

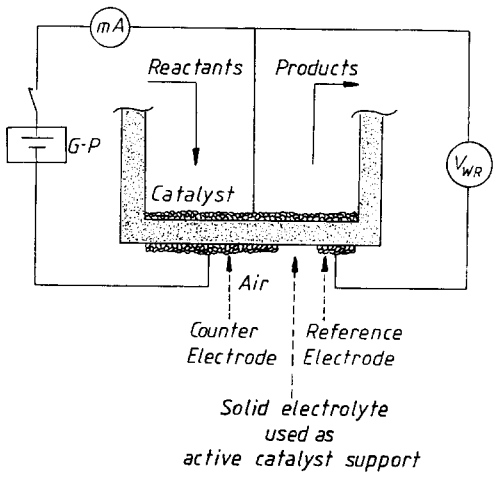

FIG. 1. Schematic of catalyst film and counter and reference electrodes; G–P, galvanostat–potentiostat.

The present work examines in detail the NEMCA effect for ethylene epoxidation on Ag deposited on 8 mol% Y_2O_3-doped ZrO_2, an O^{2-} conductor. Results of a parallel study of ethylene epoxidation on Ag deposited on β''-Al_2O_3, a Na^+ conductor, will appear elsewhere (*39*). The cell used is of the same general type used in the study of Stoukides and Vayenas (*18, 19*). It must be emphasized that in that exploratory study the catalyst overpotential η and catalyst potential V_{WR} could not be measured, due to the lack of a reference electrode. For the same reason, electrokinetic parameters of crucial importance in the description of NEMCA, such as the catalyst–solid electrolyte exchange current I_0, could not be determined. In the present study a three-electrode system is used (Fig. 1). This configuration together with the current interruption technique (*26, 37*) permits exact measurement of η, V_{WR}, $\Delta e\Phi$, and I_0. It is shown that ethylene epoxidation exhibits electrophobic behavior, but ethylene oxidation to CO_2 exhibits both electrophobic ($\Lambda > 0$) and electrophilic ($\Lambda < 0$) behavior over different V_{WR} and $e\Phi$ ranges. Product selectivity can be

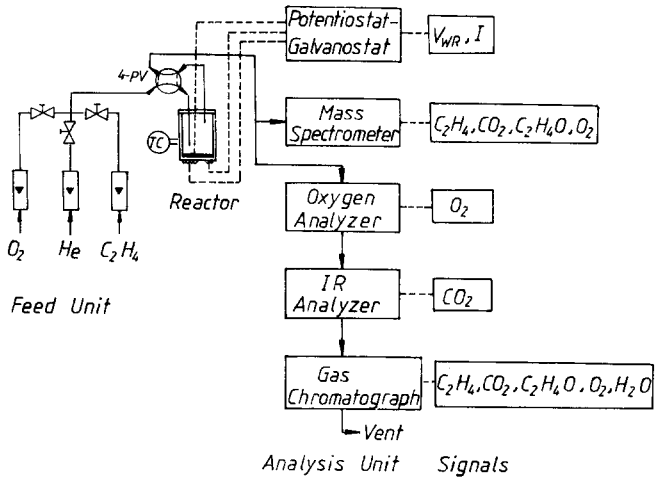

FIG. 2. Schematic of the apparatus.

influenced significantly but mostly in undesirable directions. The behavior of the system is discussed in the frame of the general theoretical model for the explanation of the NEMCA effect (*25, 37*) and also in light of recent findings of *in situ* XPS studies of Ag catalyst electrodes subject to electrochemical supply of O^{2-} (*40, 41*), i.e., subject to NEMCA conditions.

EXPERIMENTAL

The experimental apparatus utilizing on-line gas chromatography, mass spectrometry, IR spectroscopy, and an electrochemical oxygen analyzer for reactant and product analysis is shown in Fig. 2 and has been described in detail in recent studies (*25, 26, 37*).

Reactants were Messer Griesheim certified standards of C_2H_4 in He and O_2 in He. They could be further diluted in ultrapure 99.999% He (L'Air Liquide).

For the gas chromatographic analysis a Porapak N (80/100, 10 ft × $\frac{1}{8}$ in.) packed column was used to separate O_2, CO_2, and C_2H_4 at 40°C, as well as C_2H_4O and H_2O at 120°C. The O_2 concentration was also measured using a Molecular Sieve 5A (80/100, 6 ft × $\frac{1}{4}$ in.) packed column at 50°C and was continuously monitored in the exit stream by means of a Teledyne 326 RA oxygen electrochemical analyzer.

On-line mass spectrometry permitted continuous monitoring of the exit concentration of C_2H_4 (at AMU 28), C_2H_4O (at AMU 29, as CHO^+), CO_2 (at AMU 22, as CO_2^{2+}), as well as of the sum of C_2H_4O and CO_2 exit concentrations (at AMU 44). The contribution at AMU 44 due to $C_2H_4O^+$ was very small because of the low selectivity values and could be ignored to a first approximation. The cracking patterns and the relative intensities of the fragments for certified standards of the reactants and products were determined and used for quantitative analysis.

The concentration of CO_2 in the product stream was also monitored using on-line IR spectroscopy (Beckman 864). This gave a higher sensitivity to the effluent CO_2 than mass spectrometry, where the most intense CO_2 signal at AMU 44 is superimposed to the $C_2H_4O^+$ signal and to the unavoidable vacuum system background noise.

The carbon mass balance closure in all runs was better than 2%. No coking of the catalyst was detected.

The atmospheric pressure yttria-stabilized zirconia continuous-flow reactor shown schematically in Fig. 2 has been de-

scribed in detail previously (*25–37*). It has a volume of 30 cm^3 and behaves as a CSTR in the flow range 50–200 cm^3 STP/min used in this investigation, as has been shown by determination of its residence time distribution using the IR CO_2 analyzer (*20, 42*). The reactor was checked for the absence of internal and external mass transfer limitations under the conditions of the experiments (*42*). The conversion of the reactants under open- or closed-circuit conditions never exceeded 3%; i.e., the reactor was operated as a differential one. The rate of ethylene oxide oxidation was thus kept to negligible levels (*20, 42*).

The porous Ag catalyst films were deposited on the inside and outside bottoms of the stabilized zirconia tubes by application of thin coatings of a G.C. Electronics Ag suspension in butyl acetate, followed by drying and calcining in air, first at 400°C for 2 h and then at 630°C for 6 h. Porous silver catalyst films deposited in this mode have thicknesses on the order of 5–10 μm and have been shown by AES (*43*) to contain no detectable metal impurities. A typical scanning electron micrograph of the top side of a porous catalyst film used in this study is presented in Fig. 3, together with a section perpendicular to the catalyst–solid electrolyte interface.

All catalyst films used in this study have shown practically the same kinetic and NEMCA behavior. Their reactive oxygen uptake and exchange current values are presented in Table 1. The reactive oxygen uptakes, or catalyst surface areas, were measured using surface titration of oxygen with C_2H_4 as described in detail elsewhere (*31, 37, 43*). The values of the exchange current were measured electrochemically as described below.

Electrochemical measurements. As shown in Fig. 1, the catalyst-working electrode was deposited on the inside bottom wall of the stabilized zirconia tube, while two other porous Ag films were deposited on the ambient air exposed outside bottom. These served as the counter and reference electrodes of the thus-formed solid electrolyte cell reactor. The superficial surface areas of the working, counter, and reference electrodes were 2.0, 1.2, and 0.1 cm^2, respectively. Under closed-circuit conditions this three-electrode system configuration permitted determination of the catalyst solid electrolyte activation overpotential $\eta = V_{WR} - V^{o}_{WR}$, where V_{WR} is the ohmic-drop-free catalyst potential, i.e., the catalyst potential V'_{WR} relative to the reference electrode minus the corresponding ohmic component, and V^{o}_{WR}, is the open-circuit emf value ($V^{o}_{WR} = V_{WR(I=0)}$). This ohmic component was measured using the current interruption technique in conjunction with a Hameg HM 205 memory oscilloscope (*26, 37*). This ohmic component is proportional to the applied current I and was found to be less than 150 mV even for the highest current values used. The relation between overpotential η and current I was determined by using an AMEL 553 galvanostat–potentiostat. From this experimental relation and by using the classical Butler–Volmer equation the values of the exchange current I_0 and the anodic and cathodic transfer coefficients α_a and α_c were determined, as described in detail elsewhere (*26, 37*). These parameters are of crucial importance in understanding the electrocatalytic behavior of the catalyst–gas–solid electrolyte system (*26, 37*) as well as the electrocatalytically induced change in catalytic activity (*25, 26, 37*).

RESULTS

Open-circuit kinetics. The kinetics of ethylene epoxidation and nonselective oxidation to CO_2 were investigated first under open-circuit conditions ($I = 0$). The partial pressures of oxygen P_{O_2} and ethylene $P_{C_2H_4}$ were varied between 3 and 16 kPa for O_2 and between 0.3 and 2.3 kPa for C_2H_4. As shown in Fig. 4 both the rate of epoxidation $r_{C_2H_4O}$ and the nonselective, or deep, oxidation to CO_2 r_{CO_2} (both expressed in moles C_2H_4 consumed per second) can be adequately described by

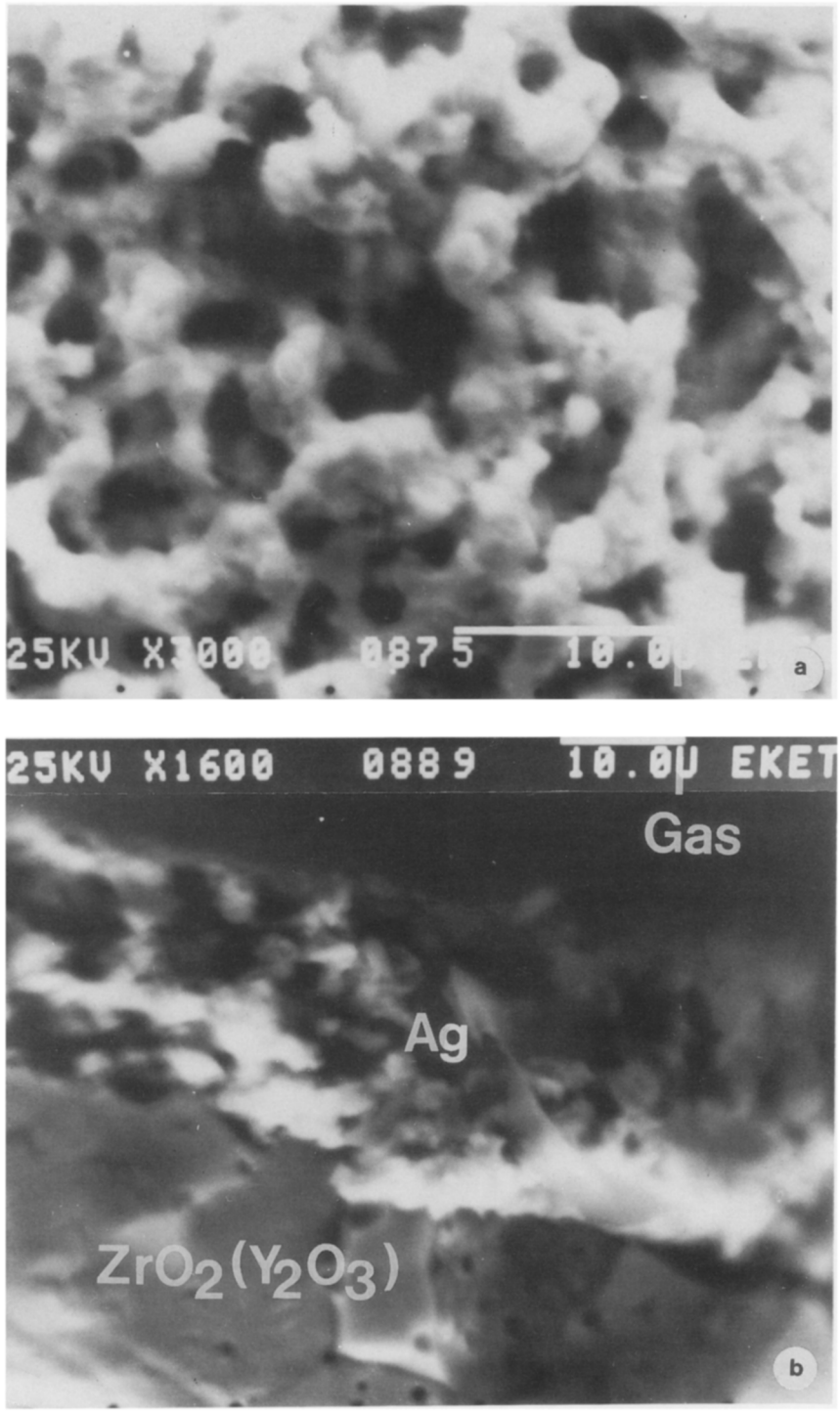

FIG. 3. Scanning electron micrographs of the top side of a Ag catalyst film (a) and of a section perpendicular to the Ag–solid electrolyte interface (b).

TABLE 1

Catalyst	Reactive oxygen uptake of catalyst N/g-atom O	Exchange current, $I_0/\mu A$ (P_{O_2} = 3.1 kPa, $P_{C_2H_4}$ = 2.4 kPa)			
		368°C	398°C	436°C	470°C
C1	4.3×10^{-8}	—	55	160	475
C2	3.8×10^{-8}	22	56	139	—
C3	2.2×10^{-8}				

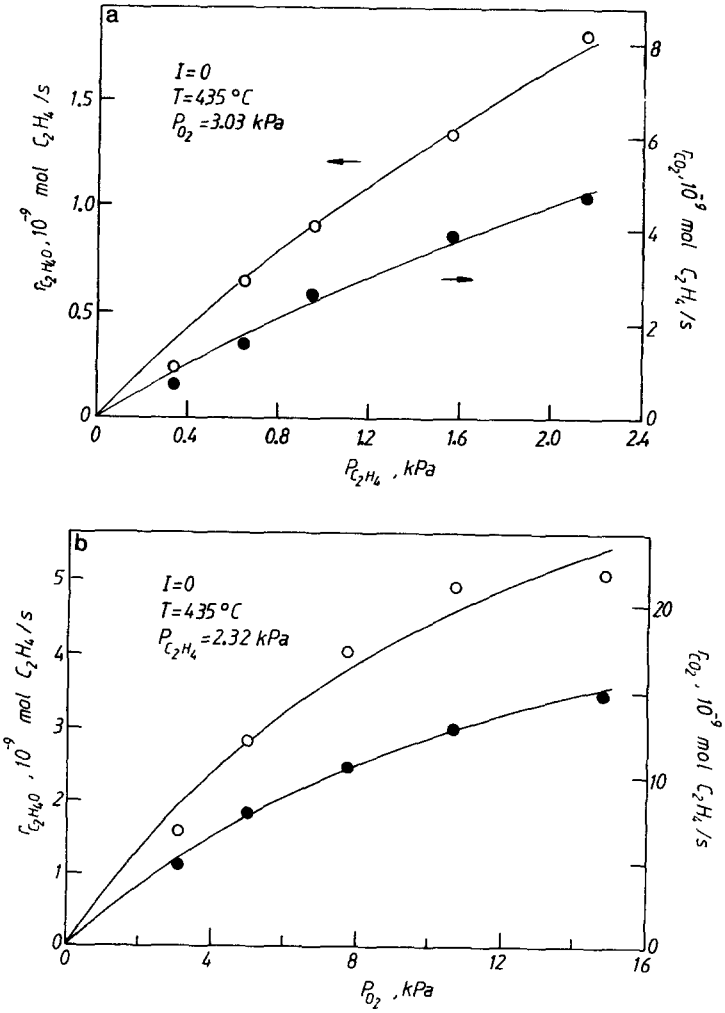

FIG. 4. Open-circuit rate dependence on $P_{C_2H_4}$ at constant P_{O_2} (a) and on P_{O_2} at constant $P_{C_2H_4}$ (b); catalyst C3; solid lines from Eqs. (6) and (7).

$$r_{C_2H_4O} = k_{C_2H_4O}(K_{C_2H_4}P_{C_2H_4}/(1 + K_{C_2H_4}P_{C_2H_4})) \cdot (K_{O_2}P_{O_2}/(1 + K_{O_2}P_{O_2})) \quad (6)$$

$$r_{CO_2} = (k_{CO_2}/k_{C_2H_4O})r_{C_2H_4O}. \quad (7)$$

These Langmuir-type rate expressions are almost identical to those reported by Stoukides and Vayenas (*20, 21*) and by Baiker *et al.* (*44*) with $K_{C_2H_4} = 0.154$ kPa, $K_{O_2} = 0.076$ kPa, $k_{C_2H_4O} = 1.77\ s^{-1}$, $k_{CO_2} = 4.90\ s^{-1}$ at 435°C. The solid lines on Fig. 4 result from the above rate expressions. Measured turnover frequencies were within a factor of 2 of those reported in Ref. (*21*). It is worth noting that Vannice and co-workers have recently established (*15*) that turnover frequencies for C_2H_4 epoxidation decrease significantly with decreasing crystallite size and that the turnover frequencies in Ref. (*21*), thus also in the present study, correspond to the limit of large crystallites (typically 1–2 μm (*15, 37*)).

Exchange current measurements. The values of exchange current I_0, or exchange current density $i_0 = I_0/A$, where A is the superficial catalyst/solid electrolyte interface surface area ($A \approx 2\ cm^2$), were extracted under catalytic reaction conditions from the linear (Tafel) part of the ln I vs η curves for anodic operation ($I > 0$) and are presented in Table 1. The value of I_0 is useful for predicting the enhancement factor Λ value according to Eq. (4).

Figure 5a shows a typical Tafel plot for anodic operation and Fig. 5b shows the temperature dependence of I_0, which was similar for both catalysts used and gives an activation energy of 1.13 eV/atom in good agreement with previous studies (*42, 45, 46*). From the slopes of the linear ln I vs η lines one obtains $\alpha_a = 0.23 \pm 0.03$ for the anodic transfer coefficient α_a. No direct measurement of the cathodic transfer coefficient α_c was possible from the ln$|I|$ vs $|\eta|$ curves for cathodic operation ($I < 0$), since in this case no Tafel region was obtained but, instead, limiting current behavior. This is due to the fact that, as shown in the Discussion of the NEMCA behavior of the system, oxygen dissolution and diffusion in the Ag catalyst affects the electrokinetic behavior. Details of the electrokinetic behavior of this system under O_2, C_2H_4, and O_2/C_2H_4 atmospheres will appear elsewhere (*47*). From the catalytic viewpoint of the present study only the I_0 values (given in Table 1) are relevant.

Due to the large I_0 values of the Ag/ZrO_2 (8 mol% Y_2O_3) interface in comparison with the I_0 values of similar Pt/ZrO_2 (8 mol% Y_2O_3) interfaces over the same temperature range (*42*) and also due to the much higher catalytic rate r_o values for C_2H_4 oxidation on Pt vs on Ag, one expects on the basis of Eq. (4) significantly lower Λ values in the present study than in C_2H_4 oxidation on Pt (*25*). This is indeed the case as shown below.

NEMCA behavior: Transients. Figure 6a shows a typical galvanostatic transient, i.e., a typical catalytic rate and catalyst potential response upon imposition of a positive current I between the counter electrode and the catalyst, so that a flux of O^{2-} equal to $I/2F$ is constantly supplied to the catalyst after $t = 0$.

At the start of the experiment the electrical circuit is open and the rates of epoxidation and deep oxidation are $r_{o,C_2H_4O} = 1.72 \times 10^{-9}$ mol C_2H_4/s and $r_{o,CO_2} = 4.68 \times 10^{-9}$ mol C_2H_4/s. The corresponding selectivity to epoxide is $S_o = 26.9\%$.

At $t = 0$ the galvanostat is used to apply a constant current $I = 400\ \mu A$ between the counter electrode and the catalyst with a concomitant rate of oxygen transfer to the catalyst $I/2F = 2.07 \times 10^{-9}$ g-atom O/s. Both catalytic rates $r_{C_2H_4O}$ and r_{CO_2} start increasing abruptly, go through a maximum in approximately 7 min, and within 60 min stabilize to their new steady-state values which are 51% higher for epoxidation and 77% higher for deep oxidation. The selectivity to epoxide drops to $S = 23.9\%$. The corresponding increase Δr_O in the total rate of atomic oxygen consumption ($\Delta r_O = \Delta r_{C_2H_4O} + 6\Delta r_{CO_2}$) is 22.5×10^{-9}

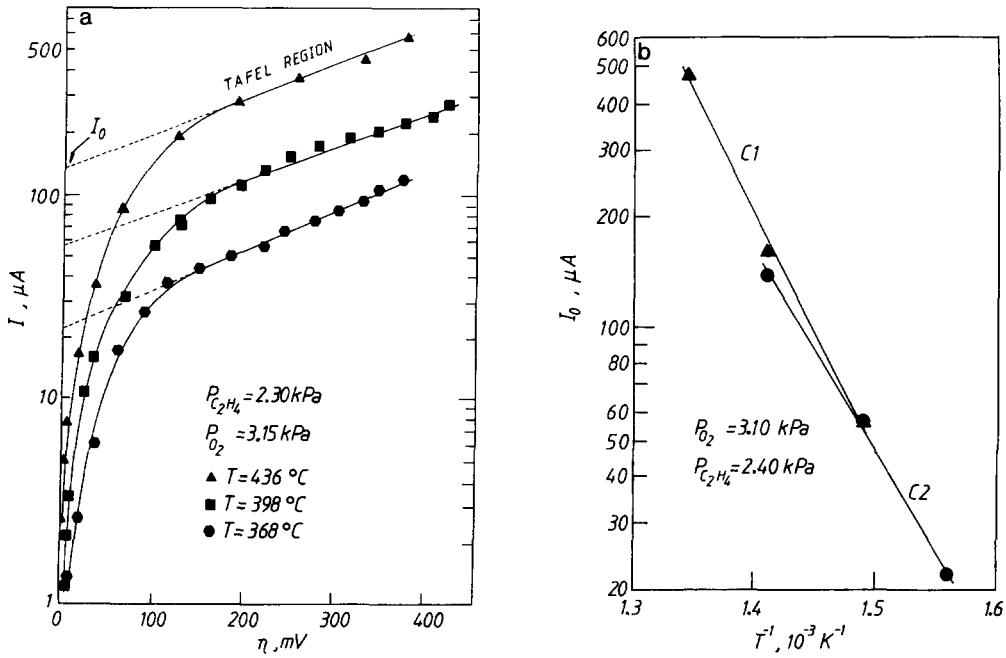

FIG. 5. (a) Dependence of anodic current ($I > 0$) on catalyst overpotential showing the Tafel region and the means of computing I_0; catalyst C2. (b) Temperature dependence of I_0.

g-atom O/s. This is near 11 times larger than $I/2F$, i.e., $\Lambda \approx 11$; thus the system exhibits NEMCA behavior.

As shown in Fig. 6a the rate transients are accompanied by a transient in catalyst potential from $V^{\circ}_{WR} = -120$ mV for $I = 0$ to $V_{WR} = +180$ mV for $I = 400$ μA. The observed changes in catalytic rates and V_{WR} are quite reversible. Upon current interruption $r_{C_2H_4O}$, r_{CO_2}, and V_{WR} all relax to their open-circuit values. The V_{WR} transient is much faster than the rate transients for this system. The origin of this type of behavior has been discussed recently (*37*).

The rate transients shown on Fig. 6a are more complex than the usual first-order-response-type rate transients obtained in previous NEMCA studies on Pt (*25*) but also on Ag surfaces at more elevated temperatures (*26*). These previously reported simple rate transients can be adequately described by taking into account the spillover of ion-compensating charge dipoles generated at the three-phase boundaries and spreading over the catalyst surface changing its work function and catalytic properties (*25, 37*). The rate transients shown in Fig. 6a and also in subsequent figures defy such a simple description. The physical origin of this complex transient behavior is analyzed under Discussion on the basis of the *in situ* XPS results obtained by Arakawa *et al.* (*40, 41*) and presented in Fig. 6b.

These authors used *in situ* XPS to examine the surface of Ag catalyst electrodes deposited on ZrO_2 (11 mol% CaO) which, like ZrO_2 (8 mol% Y_2O_3), is an O^{2-} conductor. Their experiments were very similar to the ones described here, as they examined the effect of electrochemical O^{2-} pumping to the Ag catalyst on the catalyst surface XPS spectra at temperatures 325 to 400°C and by applying current of 300 μA. Their results at 400°C are presented in Fig. 6b which is constructed from the XPS oxygen 1*s* spectra shown on Fig. 3 of Ref. (*41*): At $t < 0$, $I = 0$ and no oxygen is present on the Ag surface which is exposed to vacuum. At $t = 0$ a

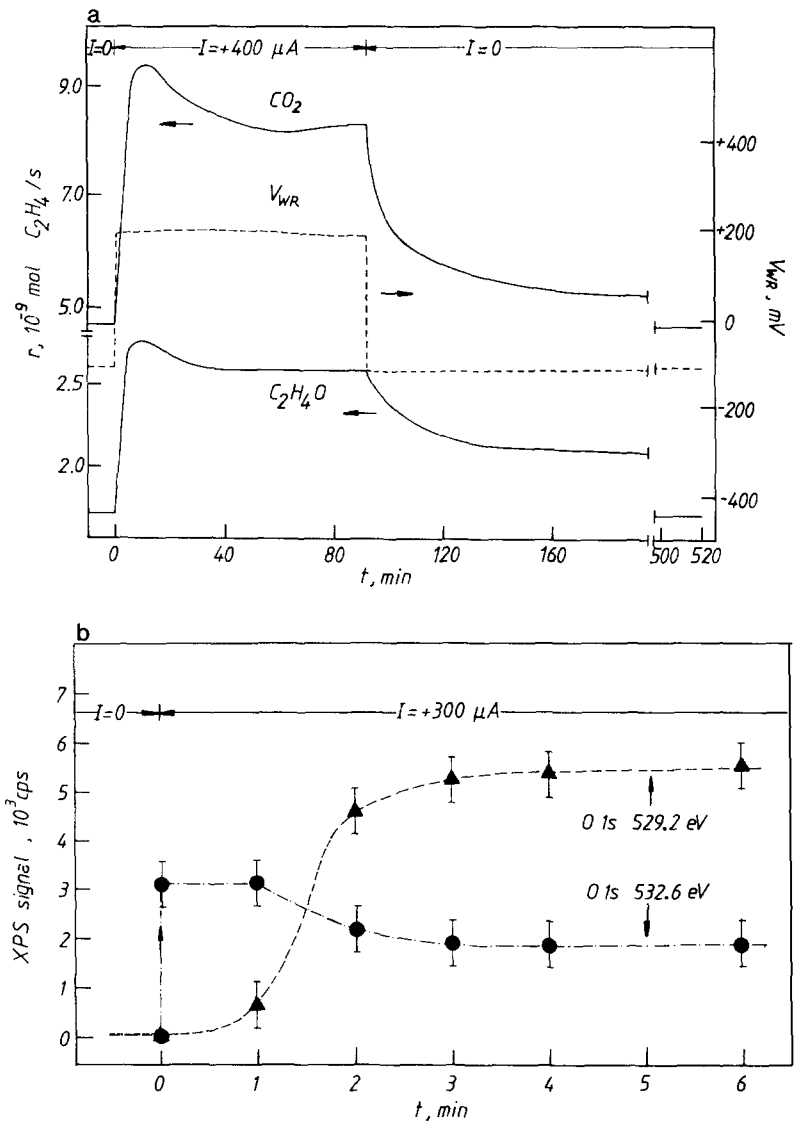

FIG. 6. (a) Rate and catalyst potential reponse to step changes in applied positive current; catalyst C3; $P_{C_2H_4}$ = 2.18 kPa, P_{O_2} = 3.09 kPa, T = 435°C; see text for discussion. (b) XPS O 1*s* signal response (peak height) to a step change in applied positive current. The peak at 532.6 eV is chemisorbed atomic oxygen and that at 529.2 eV is ionically bonded oxygen; based on the XPS spectrum of Fig. 3 of Ref. (*41*) by Arakawa *et al.* at 400°C; see text for discussion.

current I = 300 μA is applied to the cell and O^{2-} are supplied electrochemically to the catalyst. This causes the immediate appearance of an O 1*s* peak at 532.6 eV (type I, atomically adsorbed oxygen). Then after approximately 1 min another O 1*s* peak appears at 529.2 eV which gradually increases and after 3 min reaches a steady-state intensity value. This peak corresponds to ionic oxygen (*40, 41*), which must be identical to the spillover oxygen ion invoked to explain NEMCA (*22–26, 37*). Simultaneously with the increase in the intensity of the O 1*s* peak at 529.2 eV, the intensity of the O 1*s* peak

at 532.6 eV decreases by 40%. This decrease is the result of the weakening of the Ag–O bond upon increasing catalyst $e\Phi$ caused by the spillover of oxide ions (*25, 37*).

It is interesting to note the striking similarity between the rate transients (Fig. 6a) and the intensity transient of the O 1*s* peak at 532.6 eV (atomically bonded oxygen) (Fig. 6b). This similarity provides strong evidence that atomically chemisorbed oxygen is responsible both for epoxidation and for deep oxidation as already established by previous workers (*1, 11, 12*). The different time scales in Figs. 6a and 6b are due to different surface areas of the two catalyst films as shown under Discussion where the shape of the rate transients is also explained.

Figure 7a depicts a typical galvanostatic transient for $I < 0$, i.e., for O^{2-} removal from the catalyst. At $t = 0$ a current $I = -110$ μA is applied to the cell. This causes an initial abrupt decrease in both rates with a concomitant sharp decrease in V_{WR}. After a few minutes the rates, as well as V_{WR}, start to increase as they approach steady state, which corresponds to a 27% *decrease* in $r_{C_2H_4O}$ and a 12% *increase* in r_{CO_2} relative to their open-circuit values. The catalyst potential V_{WR} changes from -130 mV for $I = 0$ to -1210 mV for $I = -110$ μA.

There is a total *increase* in the rate Δr_o of atomic oxygen consumption of 3.31×10^{-9} g-atom O/s which is six times larger than the rate $I/2F$ of O^{2-} *removal,* i.e., $\Lambda = -6$. As in the case of $I > 0$ the behavior is quite reversible, i.e., $r_{C_2H_4O}$, r_{CO_2}, and V_{WR} return to their open-circuit values upon current interruption (Fig. 7a).

As shown in Fig. 7b the behavior is practically the same when the potentiostat is used to impose a step variation in V_{WR}. As expected, for an imposed value $V_{WR} = -1300$ mV the behavior of $r_{C_2H_4O}$ and r_{CO_2} is practically identical to that in Fig. 7a.

Steady-state effect of current. Figures 8a to 8e show the steady-state effect of current on the rates of epoxidation and deep oxidation and on selectivity to ethylene oxide for a $P_{O_2}/P_{C_2H_4}$ ratio of 1.3.

Increasing positive current causes up to 150% enhancement in both rates (Figs. 8a and 8b, Table 2). Enhancement factors Λ are typically on the order of 10 to 50 (maximum 100) for r_{CO_2} and 1.5 to 5 for $r_{C_2H_4O}$.

Decreasing negative currents cause a decrease of up to 30% in $r_{C_2H_4O}$ with $\Lambda_{C_2H_4O}$ values typically between 1 and 5 (Fig. 8c and Table 2). The Δr_{CO_2} behavior is more complex (Fig. 8d): A typical initial 10% decrease in r_{CO_2} is followed by a more pronounced increase of up to 40%. The behavior is strongly reminiscent of the transient r_{CO_2} behavior for $I < 0$ (Fig. 7a). The corresponding Λ_{CO_2} values are mostly in the range -3 to -50. As shown under Discussion all Λ values are in qualitative agreement with Eq. (4).

The effect of current on selectivity is depicted on Fig. 8e. Maximum selectivity is generally obtained near $I = 0$ and, depending on temperature, small increases in S can be obtained for $I > 0$ or $I < 0$. Larger positive or negative currents cause a decrease in selectivity. The effect is more pronounced for $I < 0$, where $r_{C_2H_4O}$ decreases while r_{CO_2}increases (Figs. 8c and 8d).

Effect of catalyst overpotential η. Figure 9 shows the effect of catalyst overpotential η on the rates of formation of C_2H_4O and CO_2. Both rates increase with $\eta > 0$, i.e., $I > 0$. Negative overpotentials cause a decrease in $r_{C_2H_4O}$. The rate of CO_2 formation decreases with decreasing η for $\eta > -100$ mV and then increases substantially.

As shown in Fig. 10 both $r_{C_2H_4O}$ and r_{CO_2} are exponentially dependent on η for positive η values.

Effect of catalyst potential V_{WR} *and work function* $e\Phi$. Figures 11a and 11b show the effect of V_{WR}, work function $e\Phi$, and corresponding dimensionless potential Π value ($\Pi = FV_{WR}/RT$) on $r_{C_2H_4O}$ and r_{CO_2}. As in previous NEMCA studies (*22, 37*) it is found that over wide (~0.5 eV) work function ranges the catalytic rates depend exponentially on $e\Phi$ according to

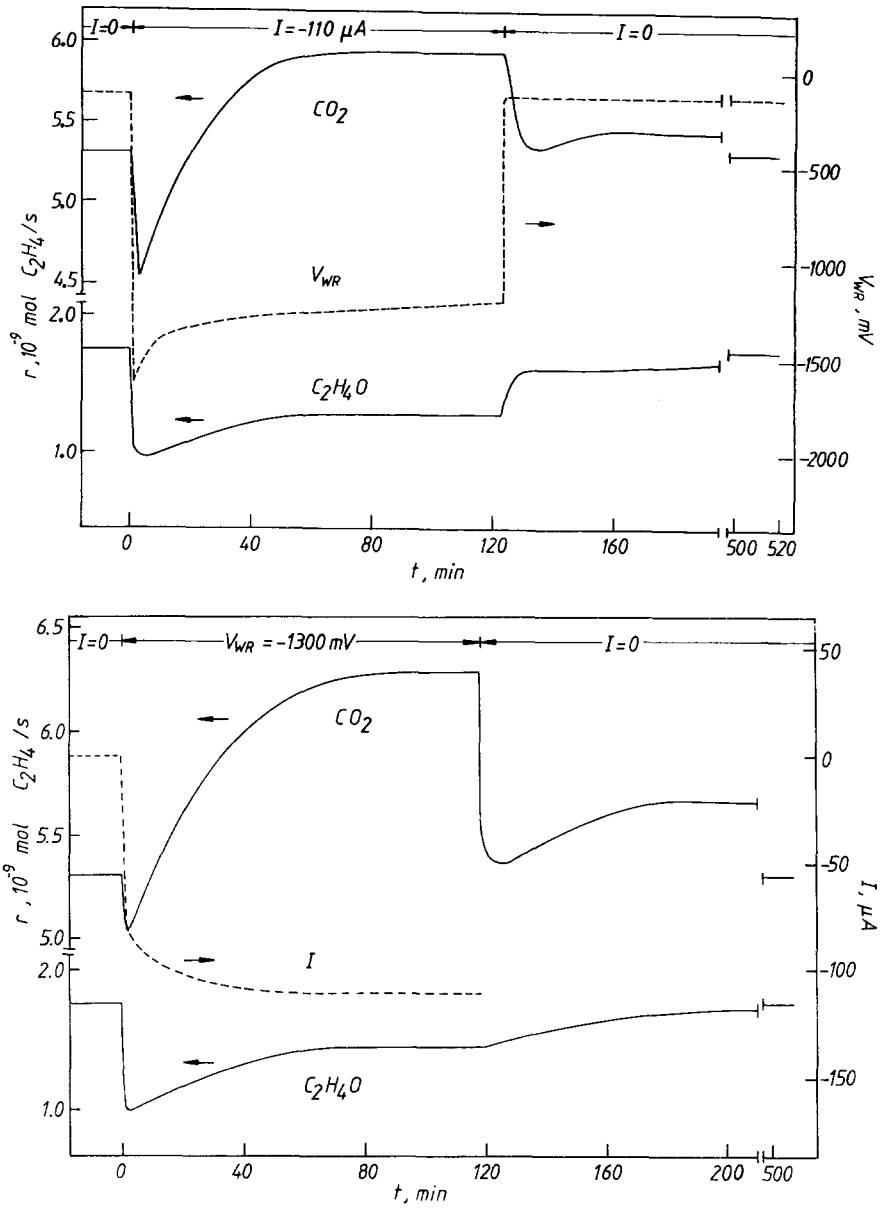

FIG. 7. (a) Rate and catalyst potential response to step changes in applied negative current; catalyst C3; $P_{C_2H_4}$ = 2.20 kPa, P_{O_2} = 3.03 kPa, T = 435°C; see text for discussion. (b) Rate and current response to a step change in catalyst potential V_{WR} (potentiostatic transient) and galvanostatic (I = 0) restoration of initial steady state; catalyst C3; conditions as in a.

$$\ln(r_{C_2H_4O}/r_{o,C_2H_4O}) = \alpha_{C_2H_4O}(e\Phi - e\Phi^*)/k_bT = \alpha_{C_2H_4O}e(V_{WR} - V^*_{WR})/k_bT = \alpha_{C_2H_4O}(\Pi - \Pi^*_{C_2H_4O}) \quad (8)$$

$$\ln(r_{CO_2}/r_{o,CO_2}) = \alpha_{CO_2}(e\Phi - e\Phi^{**})/k_bT = \alpha_{CO_2}e(V_{WR} - V^{**}_{WR})/k_bT = \alpha_{CO_2}(\Pi - \Pi^*_{CO_2}), \quad (9)$$

where $\Pi^*_{C_2H_4O} = e\Phi^*/k_bT$, $\Pi^*_{CO_2} = e\Phi^{**}/k_bT$.

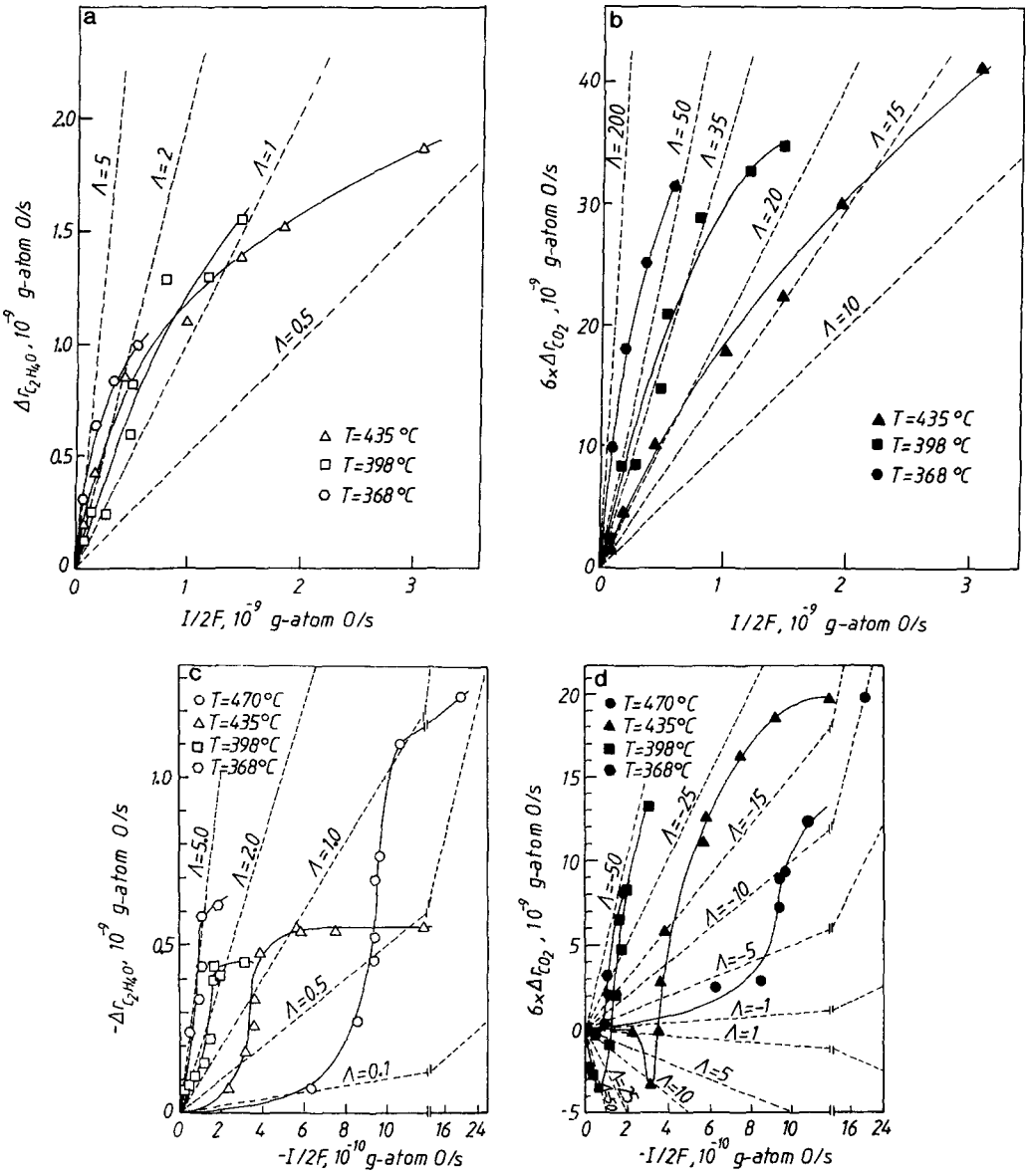

FIG. 8. Steady-state effect of applied current; catalyst C2: (a) Effect of $I > 0$ on $r_{C_2H_4O}$, $P_{C_2H_4} = 2.37$ kPa, $P_{O_2} = 3.13$ kPa. (b) Effect of $I > 0$ on r_{CO_2}; conditions as in a. (c) Effect of $I < 0$ on $r_{C_2H_4O}$; conditions as in a. (d) Effect of $I < 0$ on r_{CO_2}; conditions as in a. (e) Effect of current on selectivity; conditions as in a. Open symbols correspond to open-circuit conditions.

As shown in Figs. 11a and 11b, there exist two different regions where the above equations hold, one for high $e\Phi$ values (region I) the other for low $e\Phi$ values (region II). In region I,

$$\alpha_{C_2H_4O} = 0.08 \tag{10}$$

$$\alpha_{CO_2} = 0.12, \tag{11}$$

while in region II,

$$\alpha_{C_2H_4O} = 0.02 \tag{12}$$

$$\alpha_{CO_2} = -0.01. \tag{13}$$

The corresponding $\Pi^*_{C_2H_4O}$ values are

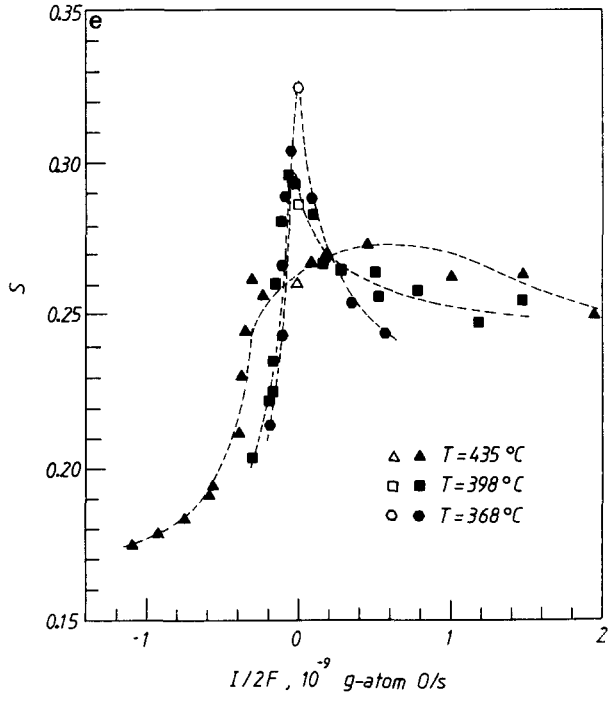

FIG. 8—*Continued*

-2.7 in region I and -2.1 in region II, while $\Pi^*_{CO_2}$ is -2.3 in region I and -1.7 in region II. The work function abscissa on Fig. 11 is constructed on the assumption that chemisorbed oxygen at near-full coverage causes an increase of 1.0 eV (*42, 48*) in the average work function of Ag with respect to vacuum conditions, taken equal to 4.50 eV (*48*).

Figure 12 shows the dependence of selectivity S on $e\Phi$ and V_{WR} for $P_{O_2}/P_{C_2H_4} = 1.3$. Decreasing $e\Phi$ causes a very pronounced, up to 60%, decrease in selectivity. As shown

TABLE 2

Open-Circuit Catalytic Rates and Turnover Frequencies (Molecules C_2H_4 Reacting/(Site · s)) at $P_{C_2H_4} = 2.40$ kPa, $P_{O_2} = 3.15$ kPa

Catalyst	T (°C)	Rates (10^{-9} mol C_2H_4/s)		TOF (s^{-1})	
		r_{o,C_2H_4O}	r_{o,CO_2}	TOF_{o,C_2H_4O}	TOF_{o,CO_2}
C1	470	7.18	18.0	0.17	0.42
	435	4.22	7.65	0.10	0.18
	398	1.89	3.67	0.04	0.09
C2	470	5.07	13.8	0.13	0.36
	435	3.12	8.82	0.08	0.23
	398	2.77	6.91	0.07	0.18
	368	2.28	4.75	0.06	0.13

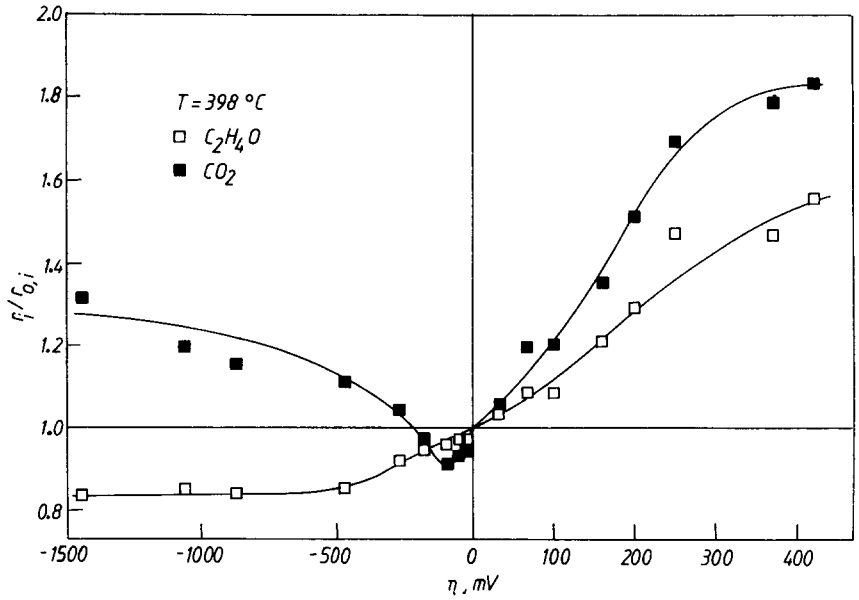

FIG. 9. Effect of catalyst overpotential η on $r_{C_2H_4O}$ and r_{CO_2} at 398°C; catalyst C2; $P_{C_2H_4}$ = 2.37 kPa, P_{O_2} = 3.13 kPa.

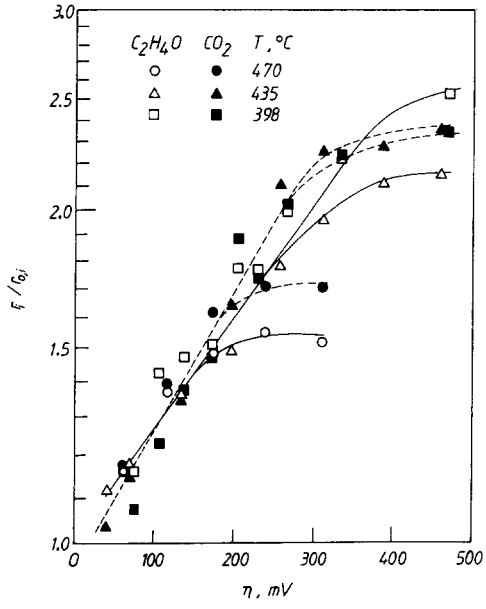

FIG. 10. Exponential dependence of $r_{C_2H_4O}$ (solid lines) and r_{CO_2} (dashed lines) on catalyst overpotential η for $\eta > 0$; catalyst C1; $P_{C_2H_4}$ = 2.48 kPa, P_{O_2} = 3.15 kPa.

in Fig. 13, selectivity is moderately dependent on gaseous composition but strongly dependent on $e\Phi$. Thus selectivity decreases from 0.22–0.26 to 0.09–0.10 upon lowering the work function $e\Phi$ by 1.3 eV.

NEMCA effect on apparent activation energies and preexponential factors. By studying the temperature dependence of $r_{C_2H_4O}$ and r_{CO_2} at constant V_{WR} (and $e\Phi$) via standard Arrhenius ln r vs T^{-1} plots, one can examine the effect of V_{WR} and $e\Phi$ on the apparent activation energies and preexponential factors of the two reactions. In the present study T was varied between 350 and 450°C at constant gaseous composition ($P_{C_2H_4}$ = 2.48 kPa, P_{O_2} = 3.15 kPa). The open-circuit activation energies were found to be $E^{\circ}_{C_2H_4O}$ = 0.78 eV and $E^{\circ}_{CO_2}$ = 0.92 eV, in good agreement with literature values (*1, 2*).

As shown in Fig. 14, increasing V_{WR} and $e\Phi$ causes a slight initial increase and then a pronounced decrease in $E_{C_2H_4O}$ and E_{CO_2}. The slopes of the $E_{C_2H_4O}$ vs $e\Phi$ plots are very close to -1. This is very similar to the observed dependence of E on $e\Phi$ during

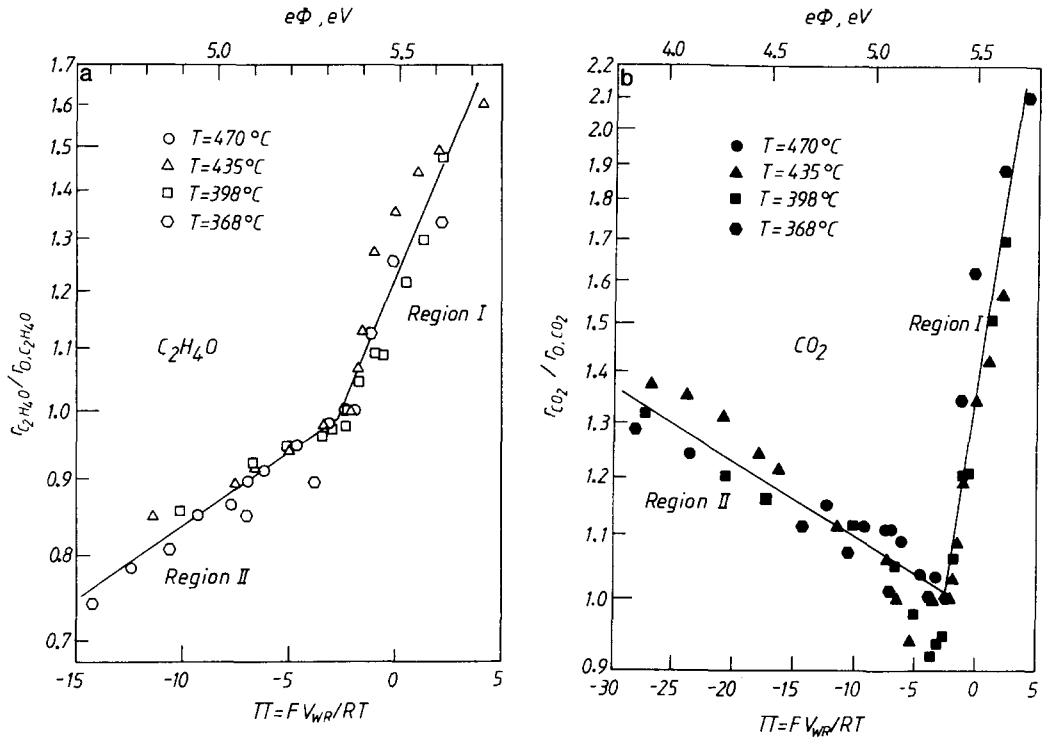

FIG. 11. Effect of catalyst potential V_{WR}, dimensionless catalyst potential Π, and catalyst work function $e\Phi$ on $r_{C_2H_4O}$ (a) and r_{CO_2} (b); catalyst C2; $P_{C_2H_4} = 2.37$ kPa, $P_{O_2} = 3.13$ kPa.

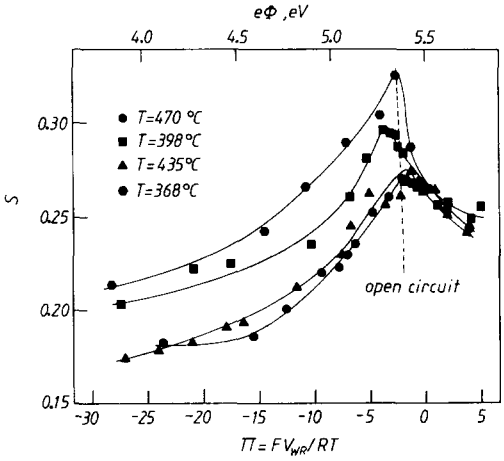

FIG. 12. Effect of V_{WR}, dimensionless catalyst potential Π, and work function $e\Phi$ on selectivity to ethylene oxide; conditions as in Fig. 11; catalyst C2.

C_2H_4 complete oxidation on Pt (*25*) which has been explained in terms of the weakening of the metal–atomic oxygen chemisorptive bond with increasing metal work function (*25, 37*). In the linear decrease region, which practically coincides with region *I* of the exponential rate vs $e\Phi$ region,

$$\Delta E_{C_2H_4O} = \alpha_{H,C_2H_4O} \cdot \Delta e\Phi \qquad (14)$$

$$\Delta E_{CO_2} = \alpha_{H,CO_2} \cdot \Delta e\Phi, \qquad (15)$$

with $\alpha_{H,C_2H_4O} = -1.03$ and $\alpha_{H,CO_2} = -0.93$.

Figure 14 also shows that this pronounced activation energy decrease is accompanied by a partially compensating decrease in the apparent preexponential factors defined from

$$k_{C_2H_4O} = k^{o}_{C_2H_4O} \exp(-E_{C_2H_4O}/k_bT) \qquad (16)$$

$$k_{CO_2} = k^{o}_{CO_2} \exp(-E_{CO_2}/k_bT), \qquad (17)$$

where the kinetic constants $k_{C_2H_4O}$ and k_{CO_2}

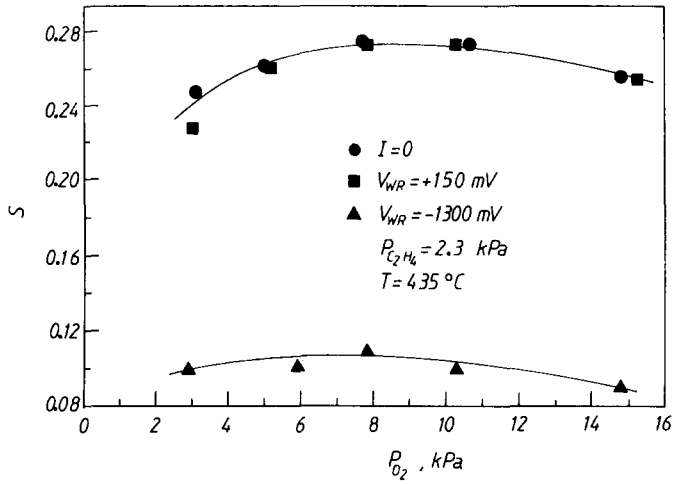

FIG. 13. Effect of gaseous composition and catalyst potential on selectivity to ethylene oxide; catalyst C3.

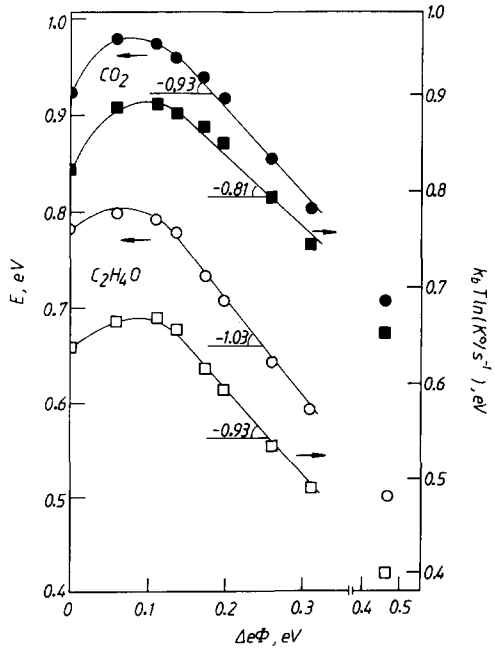

FIG. 14. Effect of catalyst work function on the activation energies and preexponential factors of epoxidation and nonselective oxidation; catalyst C1; $P_{C_2H_4}$ = 2.48 kPa, P_{O_2} = 3.15 kPa, $\Delta V_{WR} > 0$.

are obtained by fitting the data to the rate expressions (*6*, *7*). This decrease in preexponential factors can be described by

$$k_bT\ln(k^o_{C_2H_4O}/k^o_{o,C_2H_4O}) = \alpha_{S,C_2H_4O}\Delta e\Phi \quad (18)$$

$$k_bT\ln(k^o_{CO_2}/k^o_{o,CO_2}) = \alpha_{S,CO_2}\Delta e\Phi, \quad (19)$$

with $\alpha_{S,C_2H_4O} = -0.93$ and $\alpha_{S,CO_2} = -0.81$.

It should be noted that, in view of Eqs. (8), (9), and (14) through (19) it follows that, as in previous NEMCA studies (*25–37*), the following equations must hold:

$$\alpha_{C_2H_4O} = \alpha_{S,C_2H_4O} - \alpha_{H,C_2H_4O} \quad (20)$$

$$\alpha_{CO_2} = \alpha_{S,CO_2} - \alpha_{H,CO_2}. \quad (21)$$

Indeed the NEMCA coefficients $\alpha_{C_2H_4O}$ and α_{CO_2} [Eqs. (8) and (9)] were found to satisfy the above equations within 20%.

DISCUSSION

The present results show that doped zirconia solid electrolytes can be used as active catalyst supports to significantly and reversibly affect the catalytic properties of Ag for the epoxidation and deep oxidation of ethylene. Most of the findings are in qualitative

TABLE 3

Comparison of Predicted and Measured Enhancement Factor Λ Values

Catalyst	Conditions	$\Lambda_{C_2H_4O}$ (Eq. (4))	Λ_{CO_2} (Eq. (4))	$\Lambda_{C_2H_4O,exp.}$	$\Lambda_{CO_2,exp.}$
C1	T = 398°C, η = 170 mV	6.6	77.0	2.0	21.7
C2	T = 435°C, η = 125 mV	4.4	74.0	1.1	17.8
C2	T = 398°C, η = −870 mV	16.5	−82	2.7	−39.8

agreement with the earlier study utilizing a simple two-electrode system, which explored the effect of current on the catalytic rates (*18, 19*). Many of the present findings, e.g., those related to the observed magnitude of the enhancement factors Λ, can be readily explained within the framework of previous NEMCA studies (*25–37*) as discussed below. Others, such as the observed more complex rate-transient behavior and the established dependence of the rates and activation energies on catalyst potential and work function, require a more detailed discussion, as they contain useful information for the mechanism itself on the ethylene epoxidation system.

Magnitude of the enhancement factors Λ. Both C_2H_4 epoxidation and deep oxidation exhibit NEMCA, since $\Lambda_{C_2H_4O}$ values typically between 3 and 5 and Λ_{CO_2} values typically between −50 and 100 were obtained (Figs. 8a–8d). As shown in Table 3 the order of magnitude of $|\Lambda_{C_2H_4O}|$ and $|\Lambda_{CO_2}|$ can be adequately predicted by the general formula (*25, 37*):

$$|\Lambda| \approx 2Fr_o/I_0. \qquad (4)$$

The derivation of Eq. (4) has been presented in detail elsewhere (*25, 37*). Measured Λ values were typically a factor of 3 to 4 smaller than the computed ones (Table 3). This is due to the smaller values of the NEMCA coefficients $\alpha_{C_2H_4O}$ and α_{CO_2} than the anodic transfer coefficient α_a (*25, 42*). In the study of Stoukides and Vayenas (*20*) Λ values up to 300 had been measured. This can be safely attributed to a lower I_0 value of the catalyst–solid electrolyte interface in that study [Eq. (4)]. The magnitude of I_0 depends on the calcination temperature during catalyst preparation. Increasing T decreases I_0 (*25, 37*).

It is worth emphasizing (*37*) that Λ is a parameter dependent not only on the properties of the catalytic system investigated (r_o and, to a lesser extent, NEMCA coefficient α) but also on the properties of the catalyst–solid electrolyte interface (I_0 and, to a lesser extent, α_a and α_c). Thus it is a useful but not a fundamental quantity in describing NEMCA (*37*).

Catalytic rate transients and relaxation time constants τ. Previous NEMCA studies on Pt (*25*) and also on Ag, but at more elevated temperatures (*26*), have led to simple first-order-type catalytic rate transients upon imposition of constant currents (*25, 26, 37*). The more complex rate-transient behavior presently observed (Figs. 6a, 7), together with the similar transients observed independently by Arakawa and coworkers (*40, 41*) in the XPS O 1*s* signals corresponding to atomically adsorbed oxygen (532.6 eV) and ionic spillover oxygen (529.2 eV), requires and permits a more detailed tracing of the fate of O^{2-} from the time it leaves the solid electrolyte structure and is directed to the catalyst film upon imposition of a current. The observed behavior can be understood by taking into account that Ag exhibits a finite solubility for oxygen (*49*). Both the solubility of oxygen dissolved in solid Ag and its diffusivity have been measured by means of solid electrolyte cells similar to the ones employed here (*49*). This dissolved oxygen is very likely to be the same oxygen species with subsurface oxygen (*1*), the role of which on the catalytic

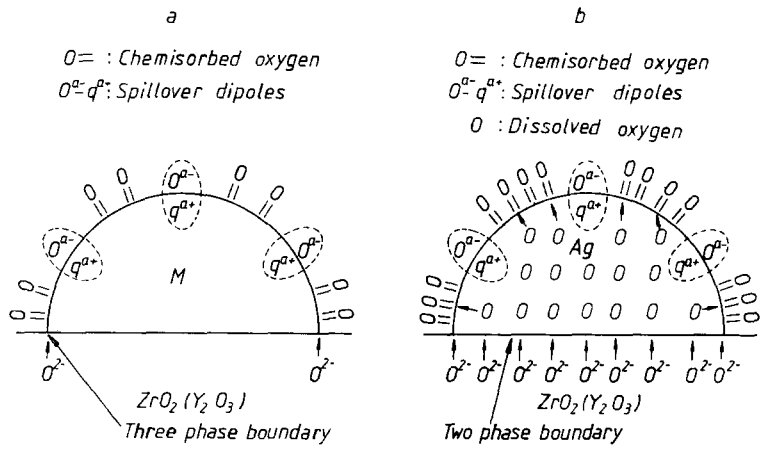

FIG. 15. Schematic of a metal crystallite deposited on stabilized zirconia, showing the oxygen pathways upon imposition of a positive current. (a) Oxygen insoluble in metal crystallites M; (b) oxygen soluble in Ag crystallites.

properties of Ag for C_2H_4 epoxidation has been studied for years (*1*). Its presence, together with the fact that oxygen can simply go through the Ag catalyst itself upon O^{2-} supply from the zirconia, must be taken into account in explaining the observed transient behavior. The situation is depicted schematically in Fig. 15

In case a (Fig. 15), applicable to metals with no appreciable solubility or diffusivity of oxygen in the bulk, i.e., practically all metals except Ag, O^{2-} can dispose of its charge only at the three-phase boundaries (tpb, metal–zirconia–gas) and form spillover dipoles, according to

$$O^{2-} \rightarrow (O^{\alpha-} - q^{\alpha+}) + 2e^- \quad (22)$$

where $O^{\alpha-}$ stands for the spillover ion (*26, 37*) of charge $\alpha-$ (there is some evidence that $\alpha = 1$ for the case of Pt (*25*)) and $q^{\alpha+}$ stands for the compensating charge in the metal. The thus-formed spillover dipoles $(O^{\alpha-} - q^{\alpha+})$ spread over the catalyst surface altering its work function and catalytic properties (*24, 25, 37*).

In addition to the charge transfer (electrocatalytic) reaction (*22*) the following electrocatalytic reaction can also take place at the tpb leading to the formation of covalently bonded chemisorbed atomic oxygen O(a) and eventually to gaseous O_2 evolution (*26, 37*):

$$O^{2-} \rightarrow O(a) + 2e^- \quad (23)$$

$$O(a) \leftrightharpoons (1/2)O_2(g). \quad (24)$$

In the case of Ag (case b, Fig. 15) in addition to the above possibilities there is a third one, i.e., charge transfer at the *two-phase boundary* of Ag–zirconia,

$$O^{2-} \rightarrow O(d) + 2e^-, \quad (25)$$

where O(d) stands for oxygen dissolved in Ag, followed by the emergence of this "subsurface" oxygen at the catalyst surface:

$$O(d) \rightarrow O(a). \quad (26)$$

It should be noted that, to the extent that the Ag crystallites are saturated with dissolved oxygen O(d), the sum of reactions (25) and (26), i.e.,

$$O^{2-} \rightarrow O(a) + 2e^-, \quad (27)$$

can occur almost instantaneously upon current application if the diffusivity of O(d) is sufficiently high. In this case its rate will be limited by the rate of supply of O^{2-} to the two-phase boundaries.

The observed transient rate and XPS signals, but also several aspects of the observed steady-state behavior, can be easily explained by taking into account that, upon current application, a fraction f_1 of the O^{2-} flux will follow pathway (22) thus leading to the formation of spillover ions, while another fraction f_2 will follow pathway (27) going through the Ag as dissolved oxygen and giving rise to an increase in the coverage of covalently bonded chemisorbed oxygen.

Thus, upon current application, dissolved "subsurface" oxygen emerges on the catalyst surface giving rise to the sharp increase in the XPS O 1*s* signal at 532.6 eV (Fig. 6b) and, simultaneously, to the observed sharp increase in the rates of epoxidation and deep oxidation (Fig. 6a).

Spillover oxide ions generated at the three-phase boundaries at a rate $f_1 I/2F$ gradually spill over the catalyst surface causing (a) the appearance of the XPS O 1*s* signal at 529.2 eV, (b) a decrease in the O 1*s* signal at 532.6 eV, and (c) a concomitant small decrease in the rates of epoxidation and deep oxidation (Figs. 6a and 6b). Thus, in a qualitative sense, the catalytic rates parallel the O 1*s* signal at 532.6 eV, i.e., covalently bonded atomic oxygen.

This observed slow and small decrease in the O 1*s* signal at 532.6 eV and in the catalytic rates, simultaneously with the observed increase in the O 1*s* signal at 529.2 eV (ionic oxygen), is in excellent agreement with the theory of NEMCA regarding the effect of spillover oxygen ions on the increase in work function and on the concomitant decrease in the strength of chemisorptive bonds (and thus also coverage) of covalently bonded electron-acceptor adsorbates, such as covalently bonded atomic oxygen (*24, 25, 30, 37*). These observations are also consistent with the findings of a recent investigation of NEMCA on oxygen chemisorption on Ag (*36*) which showed that atomic oxygen chemisorption is both enhanced and strengthened upon decreasing the catalyst work function, i.e., upon removing oxide ions from the catalyst surface (*36, 37*).

It is worth noting that the "through-the-Ag" pathway [Eqs. (25) and (26)] which results in an increase in the coverage of covalently bonded oxygen must also contribute to the $e\Phi$ increase, since covalently bonded atomic oxygen, being an electron acceptor, forms dipoles with the Ag adsorbent atoms with their negative end pointing away from the surface, i.e., it causes a negative surface potential change and thus an increase in the work function $e\Phi$. This is also manifested by the initial sharp rise in V_{WR} and thus in $e\Phi$ (Fig. 6a). Thus the role of the "through-the-Ag" pathway is not simply to provide more oxygen on the surface for reaction, but also to weaken the Ag–atomic oxygen bond via increasing $e\Phi$ along with the $e\Phi$ increase caused by the spillover ions. Thus already during the initial sharp increase in $r_{C_2H_4O}$ and r_{CO_2} (Fig. 6a) the behavior is non-Faradaic. This means not only that the coverage of adsorbed oxygen on the Ag surface has been, electrochemically, initially increased (Fig. 6b), but also that atomic oxygen on the surface has become more reactive due to the weakening of the Ag–O bond.

Regardless of the pathway followed by O^{2-} when it is supplied to the catalyst at a rate $I/2F$, upon imposition of a current I, the minimum rate relaxation time constant τ must be of the order

$$\tau \approx 2FN/I, \tag{5}$$

where N is the number of total available oxygen sites. This follows from simple mass balance considerations (*37*), provided the Ag catalyst is saturated with dissolved oxygen and that the surface diffusion of spillover dipoles is fast.

On the basis of the total reactive oxygen uptakes of the Ag catalysts used in this work, one computes from Eq. (5) $\tau = 11$ s for the rate transient on Fig. 6a and $\tau = 40$ s for the rate transient on Fig. 7a. This is in qualitative agreement with the initial transient responses but significantly slower than the secondary transient responses attrib-

uted to the spillover of oxygen ions corresponding to the O 1*s* signal at 529.2 eV. This probably indicates that the Ag catalysts were indeed saturated with dissolved oxygen, but that surface diffusion of the spillover oxygen ions is slower giving rise to the observed slower secondary rate transients.

Dependence of catalytic rates and activation energies on catalyst potential V_{WR} and work function $e\Phi$. Once the factors pertaining to the observed Λ and τ values have been rationalized, one can then concentrate on the main findings of this work, which are related to the observed dependence of catalytic rates and activation energies on V_{WR} or, equivalently, catalyst work function $e\Phi$ (Figs. 11–14).

These observations can be understood by taking into account the effect of changing $e\Phi$ on the strength of the chemisorptive bonds of the reactive surface species, i.e., covalently bonded atomic oxygen and adsorbed C_2H_4. In a very recent study (*36*) we have shown that decreasing $e\Phi$ strengthens the Ag–O chemisorptive bond in qualitative agreement with previous studies of the effect of alkali (*4–8, 10*) and chlorine promoters (*3, 6, 9*) which cause a decrease or increase, respectively, in $e\Phi$. The results of this study (*36*) are also corroborated by the experiments of Arakawa and co-workers (discussed here) which show a decrease in the amount of atomic covalently bonded oxygen upon increasing the amount of ionically bonded oxygen (Fig. 6b). It is worth mentioning that the same study (*36*) showed that changing $e\Phi$ has a minimal effect on subsurface oxygen and on adsorbed C_2H_4.

How can the observed increase in the binding strength of chemisorbed atomic oxygen (36) explain the observed decrease in activation energies with increasing $e\Phi$ and, in fact, with a slope very close to -1 (Fig. 14)? The theoretical problem of determining the change in heat of adsorption $\Delta(-\Delta H)$ of covalently bonded adatoms upon changing the substrate $e\Phi$ was originally tackled by Boudart on the basis of a simple electrostatic model (*50*). That simple model predicts

$$\Delta(-\Delta H) = -(n_e/2)\,\Delta e\Phi, \qquad (28)$$

where n_e is the number of bonding electrons. Some sign modification may be necessary in the above simple expression if one deals with electron-donor adsorbates (*30, 37*). But for electron-acceptor adsorbates, such as atomic oxygen, Eq. (28) predicts a decrease in heat of adsorption or binding strength upon increasing $e\Phi$. Similar qualitative conclusions can be reached by the more modern quantum-mechanical approaches of Shustorovich (*51, 52*) and Hoffman (*53*). For the present case, i.e., atomic oxygen adsorbed on Ag($n_e = 2$), Eq. (28) reads

$$\Delta(-\Delta H_O) = -\Delta e\Phi. \qquad (29)$$

The rate-limiting step of both C_2H_4 epoxidation and oxidation to CO_2 involves cleavage of the Ag–O chemisorptive bond. If one assumes that changing $e\Phi$ does not affect the nature of the activated complex for either reaction or the heat of adsorption of C_2H_4, the latter in good agreement with experiment (*36*), it follows then that the activation energy E of either of the two reactions must satisfy the following Polanyi type (*54*) relation:

$$\Delta E = \Delta(-\Delta H_O). \qquad (30)$$

This simplistic consideration leads to very good agreement with the observed behavior. Thus, upon combining Eqs. (29) and (30), one obtains

$$\Delta E = -\Delta e\Phi, \qquad (31)$$

which is in excellent agreement with the experiment (Fig. 14), as in the case of C_2H_4 oxidation on Pt (*25*).

The above considerations also provide an immediate explanation of the observed decrease in preexponential factors upon increasing $e\Phi$: The weakening of the Ag–O bond upon increasing $e\Phi$ increases the surface mobility of chemisorbed oxygen, thus increasing its translational partition function and, on the basis of classical transition state

theory, decreasing the preexponential factor.

The observed electrophobic exponential dependence of $r_{C_2H_4O}$ in regions I and II and of r_{CO_2} in region I, which conforms to the usual r vs $e\Phi$ dependence [Eqs. (8) and (9)], can then be immediately rationalized on the basis of the above analysis. For example for the case of epoxidation it is

$$r_{C_2H_4O} = k_{C_2H_4O}\theta_{C_2H_4O}\theta_O, \quad (32)$$

where $\theta_{C_2H_4O}$ and θ_O stand for the coverages of C_2H_4O and atomic oxygen. Since

$$k_{C_2H_4O} = k^o_{C_2H_4O} \exp[-E_{C_2H_4O}/k_bT] \quad (33)$$

$$E_{C_2H_4O} = E_{o,C_2H_4O} + \alpha_{H,C_2H_4O}\Delta e\Phi \quad (34)$$

$$k^o_{C_2H_4O} = k^o_{o,C_2H_4O} \exp[\alpha_{S,C_2H_4O}\Delta e\Phi/k_bT] \quad (35)$$

$$\alpha_{C_2H_4O} = \alpha_{S,C_2H_4O} - \alpha_{H,C_2H_4O}, \quad (36)$$

it follows that

$$\ln(k_{C_2H_4O}/k_{o,C_2H_4O}) = \alpha_{C_2H_4O}\Delta e\Phi/k_bT. \quad (37)$$

To the extent that the effect of the NEMCA-induced changes in coverages θ_O and $\theta_{C_2H_4}$ is moderate in comparison to the NEMCA-induced exponential change in the kinetic constant $k_{C_2H_4O}$, one combines Eqs. (32) and (37) to obtain the experimental Eq. (8), i.e.,

$$\ln(r_{C_2H_4O}/r_{o,C_2H_4O}) = \alpha_{C_2H_4O}(e\Phi - e\Phi^*)/k_bT. \quad (8)$$

In order to explain the observed electrophilic behavior of C_2H_4 oxidation to CO_2 in region II (Fig. 11b) and the observed dependence of the selectivity on $e\Phi$ (Fig. 12) one can take into account the model recently proposed by van Santen and Kuipers (*1*):

Ethylene epoxidation results from the reaction of adsorbed C_2H_4 with weakly bound electrophilic atomic oxygen which interacts with the π orbitals of adsorbed C_2H_4. Complete oxidation results from the interaction of more strongly bound, bridging, atomic oxygen with the C–H bond of adsorbed C_2H_4. Decreasing $e\Phi$ increases the availability of metal electrons for chemisorptive bond formation and thus enhances the surface population of the latter type of oxygen, thus enhancing CO_2 formation and decreasing the selectivity to ethylene oxide.

The observed smaller decrease in selectivity at higher $e\Phi$ values may then be the result of adsorbed ethylene reaction with spillover oxide ions which are more likely to behave like the latter type of oxygen by nucleophilically attacking the hydrogens of adsorbed C_2H_4.

Due to the low conductivity of doped ZrO_2 at temperatures below 350°C the present study was limited to high temperatures and did not involve the use of any chlorinated hydrocarbon moderators. Thus the intrinsic selectivity was low, typically 27% at 435°C, and as this study showed, could be affected by NEMCA mostly in undesirable directions.

However, the use of other types of solid electrolytes, such as β''-Al_2O_3, a Na^+ conductor, allows one to carry out NEMCA experiments at temperatures as low as 220°C, where the intrinsic selectivity of Ag is around 65% and can be increased by the addition of dichloroethylene up to 80%, i.e., near the maximum industrial selectivity values. The results of a NEMCA study under such conditions lead to technologically interesting conclusions and will be discussed elsewhere (*39*).

ACKNOWLEDGMENTS

Financial support by the EEC Non-Nuclear and SCIENCE programs is gratefully acknowledged. One of the authors (C.G.V.) thanks the Alexander von Humboldt Foundation of Germany for a fellowship.

REFERENCES

1. Van Santen, R. A., and Kuipers, H. P. C. E., *Adv. Catal.* **35,** 265 (1987).
2. Sachtler, W. M. H., Backx, C., and van Santen, R. A., *Catal. Rev. Sci. Eng.* **23,** 127 (1981).
3. Rovida, G., Pratesi, F., and Ferroni, E., *J. Catal.* **41,** 140 (1976).
4. Spencer, N. D., and Lambert, R. M., *Chem. Phys. Lett.* **83,** 388 (1981).
5. Kitson, M., and Lambert, R. M., *Surf. Sci.* **109,** 60 (1981).

6. Kitson, M., and Lambert, R. M., *Surf. Sci.* **110,** 205 (1981).
7. Peuckert, M., *Surf. Sci.* **146,** 329 (1984).
8. Tan, S. A., Grant, R. B., and Lambert, R. M., *J. Catal.* **106,** 54 (1987).
9. Campbell, C. T., *J. Catal.* **99,** 28 (1986).
10. Dean, M., and Bowker, M., *J. Catal.* **115,** 138 (1989).
11. Grant, R. B., and Lambert, R. M., *J. Catal.* **92,** 364 (1985).
12. Tan, S. A., Grant, R. B., and Lambert, R. M., *J. Catal.* **104,** 156 (1987).
13. Gleaves, J. T., Sault, A. G., Madix, R. J., and Ebner, J. R., *J. Catal.* **121,** 202 (1990).
14. Van den Hoek, P. J., Baerends, E. J., and van Santen, R. A., *J. Phys. Chem.* **93,** 6469 (1989).
15. Seyedmonir, S. R., Plischke, J. K., Vannice, M. A., and Young, H. W., *J. Catal.* **123,** 534 (1990).
16. Vayenas, C. G., *Solid State Ionics* **28–30,** 1521 (1988).
17. Stoukides, M., *Ind. Eng. Chem. Res.* **27,** 1745 (1988).
18. Stoukides, M., and Vayenas, C. G., *J. Catal.* **70,** 137 (1981).
19. Stoukides, M., and Vayenas, C. G., *ACS Symp. Ser.* **178,** 181 (1982).
20. Stoukides, M., and Vayenas, C. G., *J. Catal.* **69,** 18 (1981).
21. Stoukides, M., and Vayenas, C. G., *J. Catal.* **82,** 45 (1983).
22. Vayenas, C. G., Bebelis, S., and Ladas, S., *Nature (London)* **343,** 625 (1990).
23. Yentekakis, I. V., and Vayenas, C. G., *J. Catal.* **111,** 170 (1988).
24. Vayenas, C. G., Bebelis, S., and Neophytides, S., *J. Phys. Chem.* **92,** 5083 (1988).
25. Bebelis, S., and Vayenas, C. G., *J. Catal.* **118,** 125 (1989).
26. Neophytides, S., and Vayenas, C. G., *J. Catal.* **118,** 147 (1989).
27. Lintz, H.-G., and Vayenas, C. G., *Angew. Chem.* **101**(6), 729 (1989); *Angew. Chem. Int. Ed. Engl.* **28**(6), 708 (1989).
28. Vayenas, C. G., Bebelis, S., Neophytides, S., and Yentekakis, I. V., *Appl. Phys. A* **49,** 95 (1989).
29. Vayenas, C. G., Bebelis, S., and Neophytides, S., in "Studies in Surface Science and Catalysis" (C. G. Centi and P. Trifiro, Eds.), Vol. 55, pp. 643–652. Elsevier, Amsterdam/New York, 1990.
30. Vayenas, C. G., and Neophytides, S., *J. Catal.* **127,** 645 (1991).
31. Vayenas, C. G., Bebelis, S., and Despotopoulou, M., *J. Catal.* **128,** 415 (1991).
32. Ladas, S., Bebelis, S., and Vayenas, C. G., *Surf. Sci.* **251/252,** 1062 (1991).
33. Vayenas, C. G., Bebelis, S., Yentekakis, I. V., Tsiakaras, P., and Karasali, H., *Platinum Met. Rev.* **34,** 122 (1990).
34. Vayenas, C. G., Bebelis, S., Yentekakis, I. V., Tsiakaras, P., Karasali, H., and Karavasilis, Ch., *ISSI Lett.* **2,** 5 (1991).
35. Vayenas, C. G., Bebelis, S., and Kyriazis, C., *Chemtech* **21,** 500 (1991).
36. Bebelis, S., and Vayenas, C. G., *J. Catal.* **138,** 570 (1992).
37. Vayenas, C. G., Bebelis, S., Yentekakis, I. V., and Lintz, H.-G., *Catal. Today* **11**(3), 303–442 (1992).
38. Pritchard, J., *Nature (London)* **343,** 592 (1990).
39. Karavasilis, Ch., Bebelis, S., and Vayenas, C. G., in preparation.
40. Arakawa, T., Saito, A., and Shiokawa, J., *Chem. Phys. Lett.* **94,** 250 (1983).
41. Arakawa, T., Saito, A., and Shiokawa, J., *Appl. Surf. Sci.* **16,** 365 (1983).
42. Bebelis, Ph.D. thesis, University of Patras, 1989.
43. Stoukides, M., and Vayenas, C. G., *J. Catal.* **64,** 18 (1980).
44. Dettwiler, H. R., Baiker, A., and Richarz, W., *Helv. Chim. Acta* **62,** 1689 (1979).
45. Wang, D. Y., and Nowick, A. S., *J. Electrochem. Soc.* **126**(7), 1166 (1979).
46. Arakawa, T., Saito, A., and Shiokawa, J., *Denki Kagaku* **50**(11), 924 (1982).
47. Bebelis, S., and Vayenas, C. G., in preparation.
48. Hölzl, J., and Schulte, F. K. *in* "Solid Surface Physics," pp. 1–150. Springer-Verlag, Berlin, 1979.
49. Ramanarayanan, T. A., and Rapp, R. A., *Metall. Trans.* **3,** 3239 (1972).
50. Boudart, M., *J. Am. Chem. Soc.* **74,** 3556 (1952).
51. Shustorovich, E., *Surf. Sci. Reports* **6,** 1 (1986).
52. Shustorovich, E., *J. Mol. Catal.* **54,** 307 (1989).
53. Hoffmann, R. "Solids and Surfaces: A Chemist's View of Bonding in Extended Structures." VCH Publishers, New York, 1988.
54. Boudart, M., and Djéga-Mariadassou, G., "Kinetics of Heterogeneous Catalytic Reactions," p. 121. Princeton Univ. Press, Princeton, NJ, 1984.